Ion Mobility Spectrometric Investigation of Aromatic Cations in the Gas Phase

Toralf Beitz, Robert Laudien, and Hans-Gerd Löhmannsröben*

Universität Potsdam, Institut für Chemie, Physikalische Chemie, Karl-Liebknecht-Str. 24−25, D-14476 Potsdam-Golm

Bernd Kallies

Konrad-Zuse-Zentrum für Informationstechnik Berlin, Takustr. 7, D-14195 Berlin

Received: September 20, 2005; In Final Form: November 21, 2005

In this work, ion mobility (IM) spectra of more than 50 aromatic compounds were recorded with a laser-based IM spectrometer at atmospheric pressure. IM spectra of PAH in the laser desorption experiment show a high complexity resulting from the occurrence of monomeric, dimeric, and oligomeric cluster ions. The mobilities of all compounds were determined in helium as drift gas. This allows the calculation of the diffusion cross sections (Ω_{calc}) on the basis of the exact hard sphere scattering model and their comparison with the experimentally determined diffusion cross sections (Ω_{exp}). Extended $\Omega_{exp}/\Omega_{calc}$ and Ω_{exp}/mass correlations were performed in order to gain insight into conformational properties of cationic alkyl benzenes and internal rotation of phenyl rings in aromatic ions. This is demonstrated with some examples, such as the evaluation of the dihedral angle of the ions of 9,10-diphenylanthracene, *o*- and *m*-terphenyl, and 1,2,3- and 1,3,5-triphenylbenzene. Furthermore, sandwich and T-structures of dimeric PAH cations are discussed. The analysis was extended to oligomeric ions with up to nine monomer units. Experimental evidence is presented suggesting the formation of π-stacks with a transition toward modified π-stacks with increasing cluster size. The distance between monomeric units in dimeric and oligomeric ions was obtained.

Introduction

Ion mobility (IM) spectrometry is an important tool in physical chemistry for the investigation of ion−molecule interactions. The method is based on the drift movement of molecular ions in a bath gas under the influence of an external electrical field. The mobilities of gas-phase ions depend on the interaction potentials and the geometries of the colliding partners,[1,2] e.g., molecular cations and drift gas atoms. Hence, IM spectrometry allows experimental determination of diffusion cross sections (DCS) and structural evaluation of gas-phase ions and ionic clusters. Combined with quantum chemical calculation methods, providing structure proposals, and with improved models for DCS calculations,[3,4] a powerful tool for structure determination of gas-phase ions has been established.[5] It is based on the comparison of experimentally determined DCS (Ω_{exp}) with calculated DCS (Ω_{calc}). In connection with mass spectrometry, the method has already successfully been applied for investigations of the formation and structure of carbon clusters,[4,6] as well as for the elucidation of the structures of protein, semiconductor, and metal cluster ions.[7−13]

Considerable work has been devoted to the spectroscopy of neutral molecules and clusters in the gas phase. Molecules and clusters can be generated and investigated in supersonic beams by different spectroscopic high-resolution techniques, including resonance-enhanced multiphoton ionization (REMPI), fluorescence, and stimulated Raman spectroscopy.[14] In comparison, the number of studies addressing gas-phase structures of molecular ions and ionic clusters is still limited. Among the methods dealing with ionic clusters are photodissociation studies,[15] and the combination of photoelectron spectroscopy, mass spectrometry, and quantum chemical calculations.[16−20] But only in few cases direct experimental geometric structure information was obtained. One characteristic example is the elucidation of internal rotation in aromatic molecules. Studies for torsion of neutral molecules in the solid state or in supersonic beams are available,[21] including our work on jet-cooled tetracenes.[22] Much less is known about torsional angles in molecular ions.[5] A second example is the investigation of aromatic clusters. Most experimental and theoretical studies have focused on spectroscopic and structural properties of neutral aromatic clusters, which form van der Waals complexes of different geometries.[14] In these cases, the formation of dimer sandwich and T-structures with nearly equal energies is well-known. But also for trimers, tetramers, and pentamers, different structure proposals are discussed. For higher aromatic oligomers the appearance of π-stacks is assumed.[23] We have previously reported on conformational van der Waals isomers in mixed molecular clusters.[24] Again, little information is available about the corresponding ionic structures.[4,25] The transition from neutral to ionic clusters strongly increases the interaction and thus the bonding energies within the clusters.[15,26,27] This is usually accompanied by structural changes. The potential of IM spectrometry as an attractive method for probing structures of aromatic ions and ionic clusters in the gas phase has been demonstrated. For example, cationic benzene clusters with 2−6 monomer units were investigated. Two parallel existing conformations for each cluster size were found experimentally, and structure proposals were obtained by quantum chemical calculations confirming the experimental data.[28−30]

* To whom correspondence should be addressed. Tel: ++493319775221. Fax: ++493319775058. E-mail: loeh@chem.uni-potsdam.de.

10.1021/jp055335n CCC: $33.50
Published on Web 02/16/2006

In this work, IM spectra of more than 50 aromatic compounds were recorded. Extended $\Omega_{exp}/\Omega_{calc}$ and Ω_{exp}/mass correlations were performed in order to gain insight into conformational properties of cationic alkyl benzenes and internal rotation of phenyl rings in aromatic ions. Furthermore, sandwich and T-structures of dimeric PAH cations are discussed. The analysis is extended to oligomeric ions with up to nine monomer units. Experimental evidence is presented suggesting the formation of π-stacks with a transition toward modified π-stacks with increasing cluster size.

Experimental Setup

The experimental setup of our laser-based IM spectrometer consists of a tunable laser as ionization source and a home-built IM spectrometer.[31] As laser system a Nd:YAG laser (Spectra Physics, Darmstadt, Germany, PRO 190-10) pumping a tunable dye laser (Sirah, Kaarst, Germany, PRSC-LG-30) was used as the MPI source. The laser beam diameter entering the IM spectrometer through a quartz glass window was about 1 mm. The laser energy at the location of the ionization region was typically in the range 10−100 μJ at excitation wavelengths of 266 and 300 nm. A home-built IM spectrometer similar to that described by Gormally et al.[32] was used in two different setups for volatile compounds (gas-phase experiment) and less volatile compounds (desorption experiment). The drift tube (drift length 10.5 cm, inner diameter 3 cm, electrical field $E = 298.5$ V cm^{-1}) consisted of alternating rings made of Teflon and stainless steel. A more detailed description of the IM spectrometer was previously published.[31,33,34] In all experiments, helium 5.0 (Messer Griesheim GmbH, Krefeld, Germany, 99.999% purity) was used as drift gas. Furthermore, a high capacity moisture trap and a high capacity carbon trap (Fa. Supelco) was used to remove all traces of water and organic compounds. The volatile compounds, which were placed in diffusion or permeation tubes, were introduced into the ionization region with helium as carrier gas (sample gas). The concentration of the sample was adjusted by appropriate dilution of the sample gas through mixing with a system of mass flow controllers (MCZ GmbH, Ober-Mörlen, Germany, MK 10) and by variation of the temperature of the sample tubes placed in an oven or a cooling bath. Gas flow rates were typically 400 mL min^{-1} for the drift gas and 150 mL min^{-1} for the sample gas. The less volatile compounds were dissolved in *n*-pentane (Roth, Karlsruhe, Germany) or tetrahydrofuran (Sigma-Aldrich, Seelze, Germany), and around 50 μL of the solution were placed on an aluminum sample holder. After evaporation of the solvent the sample holder was introduced into the IM spectrometer. Desorption and ionization of the sample was performed in a single step.

Experimental and Computational Methods

The mobility of ions in a bath gas under the influence of an electrical field depends on the geometrical structure of both partners. The theory developed by Mason et al. gives the following equation, showing an indirect proportionality between ion mobility (K) and DCS (Ω)[1]

$$K = \frac{v_D}{E} = \frac{3\sqrt{2\pi}}{16}\frac{q}{N_{Gas}}\sqrt{\frac{1}{m_{Ion}}+\frac{1}{M_{Gas}}}\frac{1}{\sqrt{k_B T}}\frac{1}{\Omega} \quad (1)$$

In this equation, v_D is the drift velocity, q the ionic charge, N_{Gas} the bath gas number density, k_B the Boltzmann constant, T the temperature, and m_{Ion} and M_{Gas} are the masses of the molecular ions and bath gas atoms. The DCS Ω is an orientationally averaged collision integral. It is pointed out that eq 1 is obtained with several simplifying assumptions and is valid only for slowly drifting ions under low E/N_{gas} conditions (low field case).[1] To facilitate comparison of experimental results obtained for different pressures and temperatures, the standard (or reduced) mobility K_0 is introduced

$$K_0 = K\frac{T_0}{T}\frac{p}{p_0} \quad (2)$$

(with reference pressure $p_0 = 1.013 \times 10^5$ Pa, reference temperature $T_0 = 273$ K; p in Pa, T in K).

Drift times of cations X^+ were measured against anisole and naphthalene cations as reference substances, eliminating daily fluctuations and reducing the standard deviation of K_0 below 1%. The naphthalene cation (naph$^+$) was used as IM standard,[35,36] i.e., the measured drift times [t_D(naph$^+$), $t_D(X^+)$] were taken to obtain $K_0(X^+)$ which was based upon K_0(naph$^+$) = 8.8 cm^2 V^{-1} s^{-1} reported by de Gouw et al.[5,36,37]

$$K_0(X^+) = \frac{t_D(\text{naph}^+)}{t_D(X^+)}K_0(\text{naph}^+) \quad (3)$$

The advantage of this procedure is that possible experimental error sources, such as temporal instability or spatial inhomogeneity of the electrical field, thermal effects on drift tube length, etc., are taken out. The calculated ion mobilities were compared with results of other authors and good agreement for the few results available for He as drift gas was found (e.g., for cationic biphenyl $K_0 = 7.63$ (this work), 7.60 and 7.90 cm^2 V^{-1} s^{-1} and *p*-terpenyl $K_0 = 5.74$ (this work) and 5.88 cm^2 V^{-1} s^{-1}).[5,36,38] With eq 1, experimental DCS values ([$\Omega_{exp}(X^+)$]) for the individual cations were then obtained from the $K_0(X^+)$ values. The number of ions produced increased strongly with enhanced laser intensity. It was found that excitation intensity, and thus ion number density, did not affect the ion mobilities. Therefore, under our experimental conditions, ion−ion interactions can be ruled out.

The calculated DCS ([$\Omega_{calc}(X^+)$]) can be obtained by averaging the momentum transfer cross section over the relative velocity and the collision geometry. The most rigorous DCS calculation for polyatomic ions using realistic potentials is extremely computationally intensive. By use of helium as drift gas with low polarizability, interactions other than collisions between molecular ion and drift gas atom can be neglected in the most cases. The atoms in molecules and clusters are approximated as hard spheres and therefore the interactions are described as collisions between hard spheres. The projection model (PM) was introduced, which determines the projection area of the molecule averaged over all collision angles. More ambitious models, such as the exact hard sphere scattering model (EHSSM) introduced by Shvartsburg and Jarrold, treat the collision process more rigorously[8]

$$\Omega = \frac{1}{4\pi^2}\int_0^{2\pi} d\theta \int_0^{\pi} d\varphi \sin\varphi \int_0^{2\pi} d\gamma \int_0^{\infty} db\, 2b(1-\cos\chi(\theta,\varphi,\gamma,b)) \quad (4)$$

In this expression the angles θ, φ, and γ define the collision geometry, $\chi(\theta,\varphi,\gamma,b)$ is the scattering angle and b is the impact factor. The EHSSM takes into account that multiple collisions can occur in concave parts of the molecule and that other regions may not all be accessible to collisions. In the case of purely convex surfaces the collision integrals of PM and EHSSM are

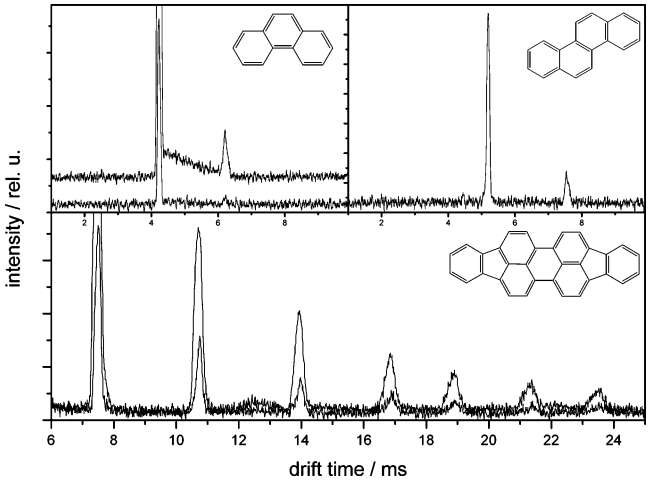

Figure 1. IM spectra of phenanthrene, chrysene, and periflanthene. For phenanthrene, the upper trace (shifted upward) was obtained at higher laser intensity.

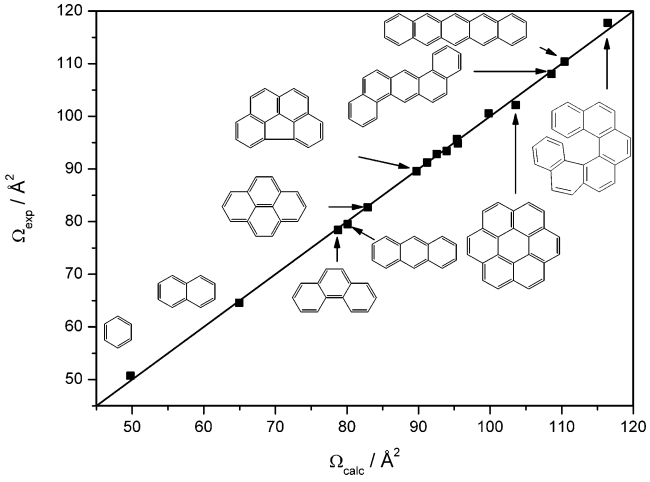

Figure 2. $\Omega_{exp}/\Omega_{calc}$ correlation for monomeric ions of 16 rigid aromatic compounds. The calculated DCS were obtained with the EHSSM; the straight line represents the ideal 1:1 identity. The size of the data points reflects approximately the experimental and computational uncertainty.

equal. In the case of concave regions the results of PM and EHSSM can deviate up to 20%. In distinction to other recommendations,[39] our experience with these molecules shows that the description by the EHSSM is better than by the PM. Therefore, only EHSSM calculations will be presented in the following. As a criterion for the correct description of a structure, measured and calculated DCS should deviate less than 2%.

Except for the cationic PAH monomers and dimers of coronene, perylene, and chrysene, the calculation of the theoretical DCS was carried out in two steps. First, a systematic conformational analysis followed by geometry optimization of the individual conformers with the UB3LYP/6-31G(d) DFT method (in some specified cases UB3LYP/3-21G*) was performed. In the next step, the DCS according to EHSSM were calculated with the program MOBCAL developed by Shvartsburg and Jarrold.[3] Geometry optimization of the cationic dimers of coronene, perylene, and chrysene was carried out using the UB3LYP/6-31G(d) DFT method.[40] Symmetry constrains in combination with manipulation of initial guesses were applied to force convergence to specific electronic states. To verify the result of a geometry optimization to be a stationary point on the potential-energy hypersurface, analytical force constants were calculated in the harmonic approximation. The structure with the lowest energy and no negative force constants was selected for further calculations. The DFT calculations were carried out using the Gaussian 03 program suite[41] on an IBM p690 Cluster (HLRN).[42]

Results and Discussion

Method Evaluation. Three examples of experimental IM spectra (phenanthrene, chrysene, periflanthene) are shown in Figure 1. For phenanthrene, one relatively sharp peak was obtained that can be assigned to the radical cation (phen$^+$, radical cations are referred to in the following simply as cations). With increasing laser intensity, a second peak at higher drift times is observed which belongs to the dimeric cation $(phen_2)^+$. The assignment of the cationic species is based on mobility/mass correlations[34] and, as shown below, on comparison of experimental and calculated DCS and DCS/mass correlations. Furthermore, the formation of the cations M^+ in the IM spectrometric laser desorption experiments at atmospheric pressure was already confirmed by mass spectrometric detection.[43] For chrysene, besides the cation peak (chry$^+$), the dimer cation was also found, however, with, in comparison to phenanthrene, significantly enhanced yield relative to the monomer ion. Shown as the third example is the IM spectrum of periflanthene (perf$^+$), containing monomeric, dimeric, and several higher oligomeric cation species [up to $(perf_7)^+$].

The maximally observed dimer/monomer ratio is about 30%. Oligomeric cations with up to nine monomeric units could be found. These three IM spectra demonstrate the tendency that the formation of larger cationic clusters correlates with molecular polarizabilities (α) of the corresponding PAH, in accordance with the Langevin potential for ion−molecule interactions.

The observation of dimers formed by monomers of lower polarizabilities becomes possible by adding, e.g., gaseous naphthalene to the drift gas as detected for the naphthalene$^+$/naphthalene complex and the anthracene$^+$/naphthalene complex (not shown). During their passage through the drift tube, the monomeric naphthalene or anthracene ions react with neutral naphthalene molecules to the corresponding complex ions, the yields of which depend on the equilibrium constant of the reactions.

The verification of calculations and experimental methods is based on the correlation of calculated and experimental DCS of PAH cations with well-defined molecular structure. Shown in Figure 2 is a plot of Ω_{exp} vs Ω_{calc} for 16 aromatic cations derived from benzene and various PAH, ranging from naphthalene over phenanthrene, anthracene to coronene, 1.2.5.6-dibenzoanthracene, pentacene, and hexahelicene.

Most of these have never been measured in IM spectrometry, and the Ω_{exp} values are reported here for the first time. The compounds are flat (apart from hexahelicene) and rigid molecules. Therefore, the DCS calculation includes only one conformation and can be easily performed. The excellent quality of the $\Omega_{exp}/\Omega_{calc}$ correlation is evident from Figure 2 (correlation coefficient R^2 from regression analysis better than 0.999, maximum deviation from 1:1 line less than 1.3%). We have previously reported on such high agreement quality $\Omega_{exp}/\Omega_{calc}$ correlations for other PAH compound classes, namely, fluoranthenes and [*n*]phenylenes.[31] The correlations of the DCS with the PAH molecular weights (DCS/mass correlations, not shown) is also very good ($R^2 = 0.9965$). It is of interest to look at the two isomeric compounds in Figure 2, anthracene (cation ant$^+$) and phenanthrene: While the experimental precision is not good enough to resolve ant$^+$ and phen$^+$, they can be distinguished with help of the calculated DCS. Clearly, isomeric substances

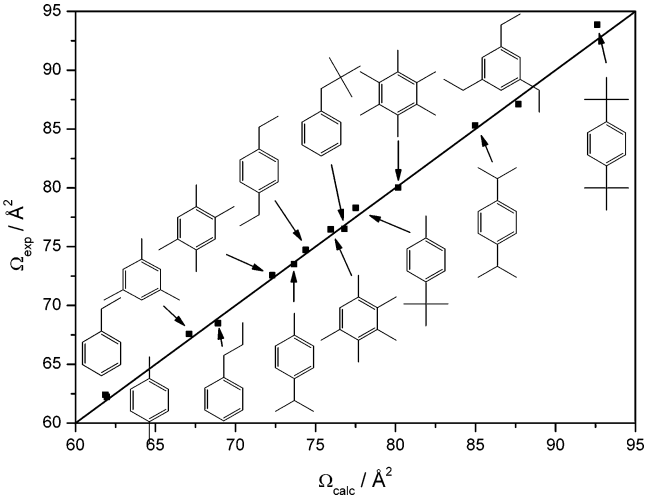

Figure 3. $\Omega_{exp}/\Omega_{calc}$ correlation for 13 "short-chain" alkyl benzenes.

cannot be identified by mobility/mass or DCS/mass correlations. In comparison to the MS techniques, the capability to distinguish isomers is a distinct feature of IM sprectrometry.

The good $\Omega_{exp}/\Omega_{calc}$ correlation for the rigid aromatic compounds provides the basis for the evaluation of another substance class, the alkyl benzenes. As new structural elements, they contain alkyl side chains, and the C/H-ratio is changed considerably. The flexibility of the alkyl chain is characterized by the large number of possible conformations between which the transformation is a very fast process in comparison to collision times. Therefore, experimentally determined drift times probe the energy-based averaged DCS of all chain conformations. Exact calculations to determine the local energy minima of the conformers could be based on molecular dynamics (MD) simulations. Such MD calculations are demanding and time-consuming, particularly if the energetic differences are very small.

First, a subset of molecules, ranging from xylene over hexamethylbenzene to di-*tert*-butyl benzene, is considered which contain methyl, ethyl, isopropyl, or *tert*-butyl groups ("short-chain" alkyl benzenes). For IM spectrometric resolution, rotation of these groups has no significant effect on DCS calculations, which are thus easily performed. As shown in Figure 3, the $\Omega_{exp}/\Omega_{calc}$ correlation for the "short-chain" alkyl benzenes is again of high quality ($R^2 = 0.9978$, maximum deviation from 1:1 line less than 1.4%). This indicates the reliability of our DCS analysis even for substances with high conformational flexibility. Together with the results for the rigid PAH presented above, the agreement between Ω_{exp} and Ω_{calc} provides a DCS "ruler" that allows the extraction of structural information, as demonstrated in the next section.

Structure Discussion and Dihedral Angles. The structure of the flexible alkyl chain of the *n*-alkyl benzenes can be described as an average of many conformations, the number of which is increasing with chain length. Figure 4 shows the $\Omega_{exp}/\Omega_{calc}$ correlation for selected short-chain and all-trans alkyl benzene cations.

For the latter, the all-trans conformations have the largest Ω_{calc}, showing stronger deviations from the 1:1 identity line with increasing chain length. These deviations are significant for the *n*-pentyl benzene cation (npbenz$^+$) and the higher homologues. Also included in Figure 4 are the DCS of the three npbenz$^+$ conformers, with the so-called scorpion, gauche, and all-trans geometries, detected by REMPI photoelectron spectroscopy in molecular beam experiments.[44] The significant

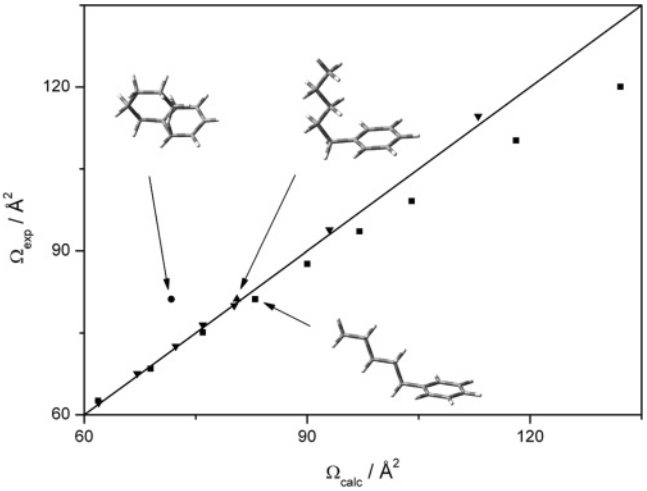

Figure 4. $\Omega_{exp}/\Omega_{calc}$ correlation for all-trans (squares) and selected short-chain alkyl benzenes (triangles). The DCS calculated for three conformations of *n*-pentyl benzene are highlighted.

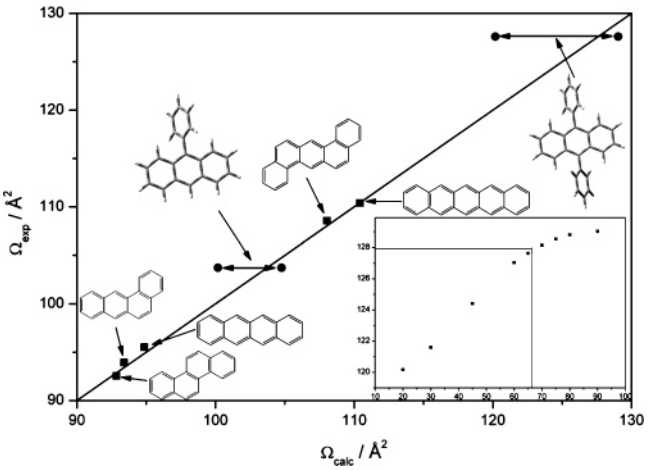

Figure 5. $\Omega_{exp}/\Omega_{calc}$ correlation for five cationic PAH (cf. Figure 2) together with $\Delta\Omega_{calc}(\Theta)$ for pant$^+$ and dpant$^+$ (horizontal arrows). The inset shows Ω_{calc} as function of the dihedral angle Θ (in degrees) for dpant$^+$.

variation of Ω_{calc} obtained for these three conformations shows impressively the potential of the DCS analysis to learn more about gas-phase structures. Our IM spectrometric results point to the conclusion that the averaged npbenz$^+$ structure, for which the gauche geometry may be one possible description, is more compact than the all-trans conformation.

Another example for the extraction of structural information, such as concerning internal rotation, of molecular ions by IM spectrometry is the determination of the dihedral angles (Θ) of aromatic molecules with side phenyl rings. For compounds with more than two aromatic moieties, the various Θ are almost identical (in absolute values) and are represented by one angle in the following. First, 9-phenylanthracene and 9,10-diphenylanthracene cations (pant$^+$, dpant$^+$) are considered. Presented in Figure 5 is the $\Omega_{exp}/\Omega_{calc}$ correlation for five cationic PAH (cf. Figure 2), together with the Ω_{calc} variation for pant$^+$ and dpant$^+$, obtained for the minimally and maximally possible angles ($20 < \Theta < 90°$).

It is obvious that the total $\Delta\Omega_{calc}(\Theta)$ variation is much larger than the deviations from the 1:1 identity found for the cationic PAH, e.g., 4.6 and 7.4% for pant$^+$ and dpant$^+$. $\Delta\Omega_{calc}(\Theta)$ is thus a good structural indicator. For dpant$^+$, the $\Omega_{calc}(\Theta)$ variation is shown in the inset of Figure 5. As indicated, comparison with Ω_{exp} gives as good approximation a dihedral

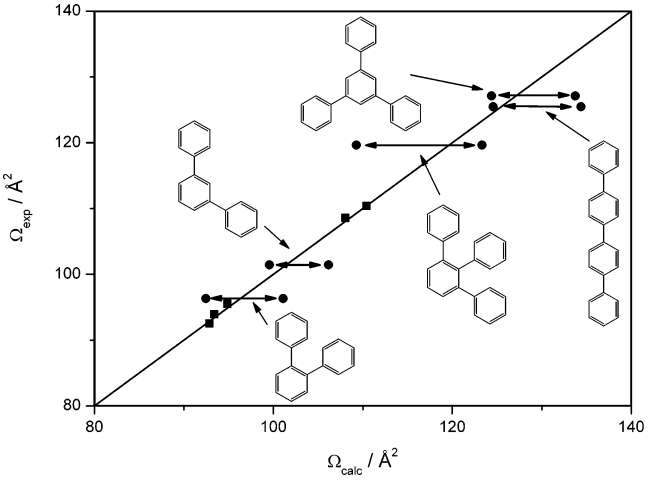

Figure 6. $\Omega_{exp}/\Omega_{calc}$ correlation for five rigid cationic PAH (cf. Figure 2) together with $\Delta\Omega_{calc}(\Theta)$ for terphenyl, triphenylbenzene, and *p,p′*-quaterphenyl cations ($10 < \Theta < 90°$).

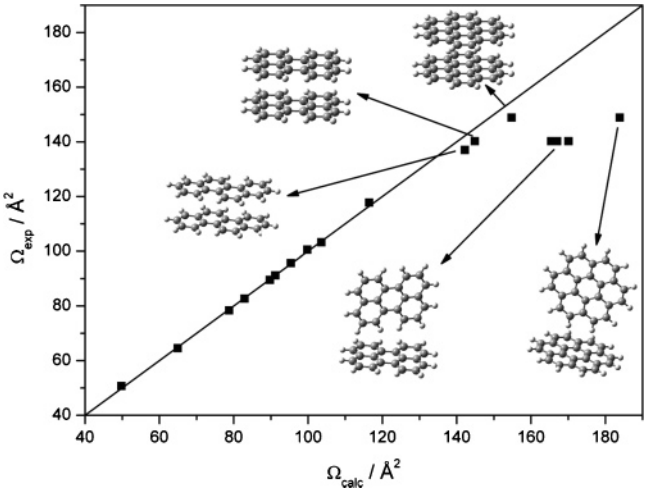

Figure 7. $\Omega_{exp}/\Omega_{calc}$ correlation for 10 PAH cations and for different structures (T and sandwich geometries) of cationic dimers for coronene, perylene, and chrysene.

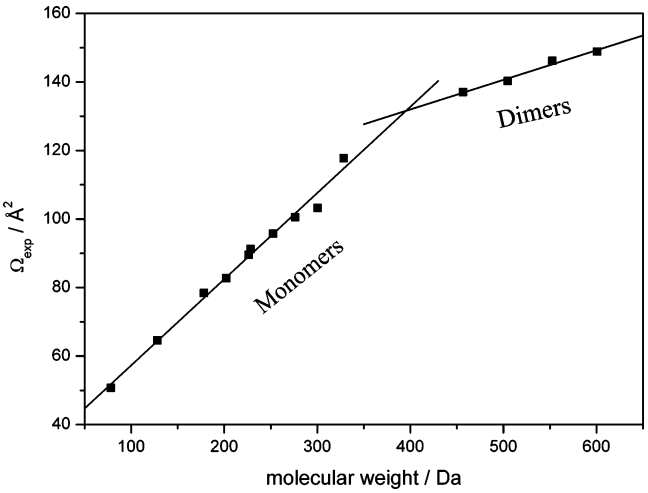

Figure 8. Ω_{exp}/mass correlation for monomeric and dimeric PAH ions.

angle of $\Theta \approx 65°$ for dpant$^+$ ($\Theta \approx 61°$ for pant$^+$). Different levels of quantum chemical calculation lead to slight changes of Θ (e.g., for dpant$^+$, B3LYP 3-21G*: $\Theta \approx 63°$).

In an IM spectrometric study, Krishnamurthy et al.[5] have determined the dihedral angle in neutral and cationic biphenyl to 40 and 17.5°, respectively. We have extended this approach to substances with three (terphenyls) and four connected phenyl rings (triphenylbenzenes, p,p′-quaterphenyl). As shown in Figure 6, the total $\Delta\Omega_{calc}(\Theta)$ ($10 < \Theta < 90°$) variations are again much larger than the deviations from the 1:1 identity, ranging from 6.4%, 8.9% for the *m*- and *o*-terphenyl cations (mtp$^+$, otp$^+$) to 7.5 and 12.9% for the 1,3,5- and 1,2,3-triphenylbenzene cations (1,3,5-tpb$^+$, 1,2,3-tpb$^+$). Evaluation with Ω_{exp} gives as good approximation dihedral angles of $\Theta \approx 36$ and 30° for otp$^+$ and mtp$^+$ and $\Theta \approx 30$ and 54° for 1,3,5-tpb$^+$ and 1,2,3tpb$^+$.

The differences in the dihedral angles of the isomers are due to steric repulsions between the phenyl rings. The free rotation of the phenyl rings in pant$^+$, dpant$^+$, otp$^+$, and 1,2,3tpb$^+$ is sterically hindered. For all compounds, the variation of Ω_{calc} with Θ are qualitatively similar to the behavior shown in Figure 5 (inset), with the highest gradient between 20 and 70°. Therefore, Θ_{exp} can be evaluated best within this interval.

Structure Discussion of Cationic PAH Dimers and Clusters. IM spectrometry is a suitable tool to contribute to the elucidation of the structures of dimeric cations. This is shown here for the dimeric cations of perylene, coronene, and chrysene, (pery$_2$)$^+$, (cor$_2$)$^+$ (chry$_2$)$^+$. In comparison to the one-dimensional consideration of the dihedral angles, the three-dimensional geometry of dimeric cations cannot be obtained in a similar simple manner. The three variables taken into consideration are the distance between the monomeric units and the parallel displacement of the monomeric units as two further independent variables. Therefore the structures can only be obtained by computationally intensive quantum chemical calculations, which provide proposals for structures with very similar lowest energies. Beside monomeric PAH cations, in the $\Omega_{exp}/\Omega_{calc}$ correlation (Figure 7), the DCS of different structures of cationic dimers (T- and sandwich structures) for (cor$_2$)$^+$, (pery$_2$)$^+$, and (chry$_2$)$^+$ are included.

For (cor$_2$)$^+$, the deviation of Ω_{calc} from the 1:1 identity line is 3% for the sandwich and 19% for the T structure. This is taken as indication that the T geometry does not play a significant role for (cor$_2$)$^+$. For (pery$_2$)$^+$, in the calculations three different T structures with very similar energies were found. These geometries can also be excluded in comparison to the sandwich structure. The good $\Omega_{exp}/\Omega_{calc}$ adherence of the sandwich stuctures, and the strong deviation of the T geometries, seem to allow the general assumption that other PAH cationic dimers are also dominated by the sandwich structure. The remaining small deviations between Ω_{exp} and Ω_{calc} for the sandwich structures can be explained with somewhat too large separation of the monomeric units resulting from the ab initio quantum chemical calculations.

Ω_{exp}/mass correlations provide a possibility to investigate the formation of cluster ions. This is demonstrated by comparison of Ω_{exp} for monomeric and dimeric ions of selected PAH in one diagram (Figure 8). Clearly, the linear regression lines of the monomeric and dimeric ions with sandwich geometries show different slopes.

Thus, the break at the interception indicates the transition from monomeric to dimeric ions. It is obvious that the DCS of a given dimeric ion is below, i.e., the mobility is above, that of a single (hypothetical) cation with the same mass. This effect is even more pronounced for larger ionic agglomerates (see below). As shown in Figure 9, the analysis of Ω_{exp} vs mass can be extended to oligomeric cations, as exemplified for coronene cluster ions (cor$_n$)$^+$ ($n = 1-5$). If the straight line from the monomeric to the dimeric cation is extrapolated, Ω_{exp} of all observed larger cluster ions are perfectly described by this line. The high linearity of the DCS/mass correlation means that

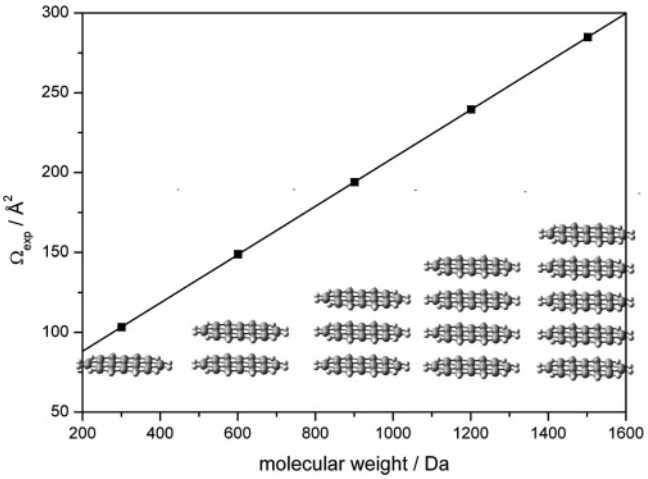

Figure 9. Ω_{exp}/mass correlation for coronene ions and schematic representation of π-stacks.

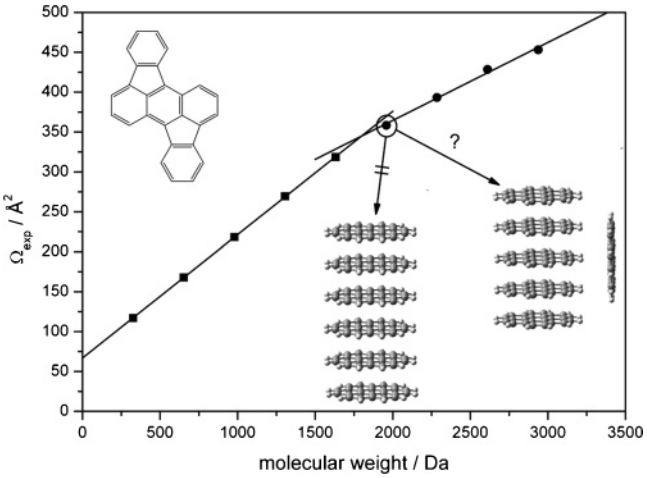

Figure 10. 10. Ω_{exp}/mass correlation for rubicene ions and schematic representation of π-stacks and modified π-stacks.

addition of another monomeric unit leads to an increase of Ω_{exp} by a constant increment. This is similar to the additivity behavior observed for spectral shifts of atomic and molecular PAH complexes in molecular beams[21] and is taken as an indication for the continuation of sandwiching as composition principle. Thus, the formation of extended π-stacks, also found for benzene cluster ions and referred to as eclipsed stacked sandwich structures,[28] is assumed (cf. Figures 9 and 10).

Analogous Ω_{exp}/mass correlations were performed for rubicene, a fluoranthene derivative, for which cluster ions with up to nine monomeric units were observed [$(rubi_n)^+$, $n = 1-9$, Figure 10]. In contrast to the coronene cluster ions, this Ω_{exp}/mass correlation shows a discontinuity. The highly linear first part, for $(rubi_n)^+$, $n = 1-5$, again indicates the formation of π-stacks. The also linear second part, starting from the hexamer ion, suggests the formation of modified π-stacks with another build-up principle. At present we can only speculate about the geometries involved, but it is tempting to assume that monomeric units are added to the sides of the π-stack cylinders (cf. Figure 10).

The analysis of Ω_{exp} vs mass was extended to further fluoranthenes. A graph including the monomeric ions of 10 fluoranthenes and all oligomeric ions of five fluoranthenes shows three different sections (Figure 11), which are proposed to belong to monomers, π-stacks and modified π-stacks. Analogous to the rubicene cations, the structure change from

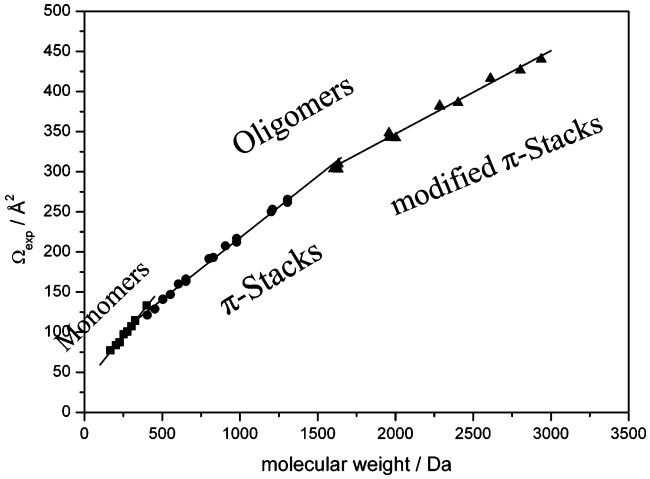

Figure 11. Ω_{exp}/mass correlation for various fluoranthenes.

π-stacks toward the modified π-stacks starts from the hexamer ion. It was previously suggested that larger benzene cationic clusters deviate from the ideal sandwich structure.[28] It seems thus possible that the build-up principle of aromatic cluster ions may be of general nature.

The distance between the monomeric units in dimeric ions and ionic π-stacks is an interesting parameter that can easily be calculated for sandwich and π-stack structures. Similar to the determination of the dihedral angles, the dependence of the DCS on the distance between the monomeric units (with averaged distance in oligomers) was calculated and correlated with Ω_{exp}. For example, separation distances of about 3.5 and 3.6 Å were obtained for $(cor_2)^+$ and $(rubi_2)^+$. The variation for different PAH and for π-stacks of different size is small and within the experimental error (ca. < 0.2 Å). Similar distances were reported for benzene cluster ions.[28]

Conclusions

In this work, IM spectra of more than 50 aromatic compounds were recorded by laser-based IM spectrometry. The mobilities of all compounds were determined in helium as drift gas and the Ω_{calc} were calculated on the basis of the EHSSM. $\Omega_{exp}/\Omega_{calc}$ correlations of different cationic PAH and alkyl benzenes demonstrate that the EHSSM provides a good description for ion−molecule interactions in helium as drift gas and indicates the reliability of theoretical model and experimental method. Therefore, the technique enables the extraction of structural information for flexible molecular ions, demonstrated with some examples, like the *n*-alkyl benzenes and the evaluation of the dihedral angle of 9,10-diphenylanthracene, *o*- and *m*-terphenyl, and 1,2,3- and 1,3,5-triphenylbenzene. Although only approximate dihedral angles were obtained, a direct method to determine structural features of molecular ions in the gas phase under ambient conditions could be presented. Such structural information was up to now not obtained otherwise. IM spectra of PAH in the laser desorption experiment show a high complexity caused by the formation of monomeric, dimeric, and oligomeric cluster ions. Extended $\Omega_{exp}/\Omega_{calc}$ and Ω_{exp}/mass correlations were performed in order to gain insight into structures of dimeric ions and higher cluster ions. Sandwich and T structures of dimeric PAH cations were evaluated. For example, the difference in the Ω_{calc} values of both structures is significant for the cationic coronene dimer (19%). The analysis was extended to oligomeric ions with up to 9 monomer units. Experimental evidence is presented suggesting the formation of π-stacks with a transition toward modified π-stacks with

increasing cluster size. The distance between monomers in dimers and oligomers was also obtained, resulting in values of about 3.5−3.6 Å.

Acknowledgment. This work was financially supported by the German Ministry of Education and Research (BMBF) in the framework of the MILAN project (FKZ: 13N8099).

References and Notes

(1) Mason, E. A.; McDaniel, E. W. *Transport Properties of Ions in Gases*; Wiley: New York, 1988.
(2) Eiceman, G. A.; Karpas, Z. *Ion Mobility Spectrometry*; CRC Press: Boca Raton, 1992.
(3) Shvartsburg, A. A.; Jarrold, M. F. *Chem. Phys. Lett.* **1996**, *261*, 86.
(4) von Helden, G.; Hsu, M.-T.; Gotts, N.; Bowers, M. T. *J. Phys. Chem.* **1993**, *97*, 8182.
(5) Krishnamurthy, M.; de Gouw, J. A.; Bierbaum, V. M.; Leone, S. R. *J. Phys. Chem.* **1996**, *100*, 14908.
(6) von Helden, G.; Hsu, M.-T.; Kemper, P. R.; Bowers, M. T. *J. Phys. Chem.* **1991**, *95*, 3835.
(7) Clemmer, D. E.; Jarrold, M. F. *J. Mass Spectrom.* **1997**, *32*, 577.
(8) Gilb, S.; Weis, P.; Furche, F.; Ahlrichs, R.; Kappes, M. M. *J. Chem. Phys.* **2002**, *116*, 4094.
(9) Jarrold, M.; Bower, J. *J. Phys. Chem.* **1993**, *97*, 1746.
(10) Shvartsburg, A.; Jarrold, M. *Chem. Phys. Lett.* **2000**, *317*, 615.
(11) Creaser, C. S.; Griffiths, J. R.; Bramwell, C. J.; Noreen, S.; Hill, C. A.; Thomas, C. L. P. *Analyst* **2004**, *129*, 984.
(12) Shvartsburg, A. A.; Hudgins, R. R.; Dugourd, P.; Jarrold, M. F. *Chem. Soc. Rev.* **2001**, *30*, 26.
(13) Collins, D. C.; Lee, M. L. *Anal. Bioanal. Chem.* **2002**, *372*, 66.
(14) Meyer, E. A.; Castellano, R. K.; Diederich, F. *Angew. Chem., Int. Ed.* **2003**, *42*, 1210.
(15) Snodgrass, J. T.; Dunbar, R. C.; Bowers, M. T. *J. Phys. Chem.* **1990**, *94*, 3648.
(16) Ohashi, K.; Nishi, N. *J. Chem. Phys.* **1998**, *109*, 3971.
(17) Saigusa, H.; Lim, E. C. *J. Phys. Chem.* **1994**, *98*, 13470.
(18) Inokuchi, Y.; Ohashi, K.; Matsumoto, M.; Nishi, N. *J. Phys. Chem.* **1995**, *99*, 3416.
(19) Song, J. K.; Lee, N. K.; Kim, S. K. *Angew. Chem., Int. Ed.* **2003**, *42*, 213.
(20) Song, J. K.; Lee, N. K.; Kim, J. H.; Han, S. Y.; Kim, S. K. *J. Chem. Phys.* **2003**, *119*, 3071.
(21) Becker, H.-D.; Langer, V.; Sieler, J.; Becker, H.-C. *J. Org. Chem.* **1992**, *57*, 1883.
(22) Löhmannsröben, H.-G.; Bahatt, D.; Even, U. *J. Phys. Chem.* **1990**, *94*, 4025.
(23) Rapacioli, M.; Calvo, F.; Spiegelman, F.; Joblin, C.; Wales, D. J. *J. Phys. Chem. A* **2005**, *109*, 2487.
(24) Löhmannsröben, H.-G.; Bahatt, D.; Even, U. *J. Phys. Chem.* **1990**, *94*, 6286.
(25) Shvartsburg, A. A.; Schatz, G. C.; Jarrold, M. F. *J. Chem. Phys.* **1998**, *108*, 2416.
(26) Meot-Ner, M. *J. Phys. Chem.* **1980**, *84*, 2724.
(27) Neusser, H. J.; Krause, H. *Chem. Rev.* **1994**, *94*, 1829.
(28) Rusyniak, M. J.; Ibrahim, Y. M.; Wright, D. L.; Khanna, S. N.; El-Shall, M. S. *J. Am. Chem. Soc.* **2003**, *125*, 12001.
(29) Ibrahim, Y.; Alsharaeh, E.; Rusyniak, M.; Watson, S.; Meot-Ner, M.; El-Shall, M. S. *Chem. Phys. Lett.* **2003**, *380*, 21.
(30) Rusyniak, M.; Ibrahim, Y.; Alsharaeh, E.; Meot-Ner, M.; El-Shall, M. S. *J. Phys. Chem. A* **2003**, *107*, 7656.
(31) Löhmannsröben, H.-G.; Beitz, T.; Laudien, R. *Proc. SPIE* **2004**, *5547*, 16.
(32) Phillips, J.; Gormally, J. *Int. J. Mass Spectrom. Ion Processes* **1992**, *112*, 205.
(33) Illenseer, C.; Löhmannsröben, H.-G.; Schultze, R. H. *J. Environ. Monit.* **2003**, *5*, 780.
(34) Illenseer, C.; Löhmannsröben, H.-G. *Phys. Chem. Chem. Phys.* **2001**, *3*, 2388.
(35) Eiceman, G. A.; Nazarov, E. G.; Stone, J. A. *Anal. Chim. Acta* **2003**, *493*, 185.
(36) Creaser, C. S.; Benyezzar, M.; Griffiths, J. R.; Stygall, J. W. *Anal. Chem.* **2000**, *72*, 2724.
(37) de Gouw, J. A.; Krishnamurthy, M.; Bierbaum, V. M.; Leone, S. R. *Int. J. Mass Spectrosc.* **1997**, *167/168*, 281.
(38) Creaser, C. S.; Benyezzar, M.; Griffiths, J. R.; Stygall, J. W. *Anal. Chem.* **2000**, *72*, 2724.
(39) Bowers, M. T. http://bowers.chem.ucsb.edu/theory_analysis/cross-sections/index.shtml (last access 17.08.2005).
(40) Becke, A. D. *J. Chem. Phys.* **1993**, *98*, 1372.
(41) Frisch, M. J.; Trucks, G. W.; Schlegel, H. B.; Scuseria, G. E.; Robb, M. A.; Cheeseman, J. R.; Montgomery, J. A., Jr.; Vreven, T.; Kudin, K. N.; Burant, J. C.; Millam, J. M.; Iyengar, S. S.; Tomasi, J.; Barone, V.; Mennucci, B.; Cossi, M.; Scalmani, G.; Rega, N.; Petersson, G. A.; Nakatsuji, H.; Hada, M.; Ehara, M.; Toyota, K.; Fukuda, R.; Hasegawa, J.; Ishida, M.; Nakajima, T.; Honda, Y.; Kitao, O.; Nakai, H.; Klene, M.; Li, X.; Knox, J. E.; Hratchian, H. P.; Cross, J. B.; Adamo, C.; Jaramillo, J.; Gomperts, R.; Stratmann, R. E.; Yazyev, O.; Austin, A. J.; Cammi, R.; Pomelli, C.; Ochterski, J. W.; Ayala, P. Y.; Morokuma, K.; Voth, G. A.; Salvador, P.; Dannenberg, J. J.; Zakrzewski, V. G.; Dapprich, S.; Daniels, A. D.; Strain, M. C.; Farkas, O.; Malick, D. K.; Rabuck, A. D.; Raghavachari, K.; Foresman, J. B.; Ortiz, J. V.; Cui, Q.; Baboul, A. G.; Clifford, S.; Cioslowski, J.; Stefanov, B. B.; Liu, G.; Liashenko, A.; Piskorz, P.; Komaromi, I.; Martin, R. L.; Fox, D. J.; Keith, T.; Al-Laham, M. A.; Peng, C. Y.; Nanayakkara, A.; Challacombe, M.; Gill, P. M. W.; Johnson, B.; Chen, W.; Wong, M. W.; Gonzalez, C.; Pople, J. A. *Gaussian 03*, revision B.05; Gaussian, Inc., Pittsburgh, PA, 2003.
(42) Norddeutscher Verbund für Hoch- und Höchstleistungsrechnen, http://www.hlrn.de (last access 19.09.2005).
(43) Young, D.; Douglas, K. M.; Eiceman, G. A.; Lake, D. A.; Johnston, M. V. *Anal. Chim. Acta* **2002**, *453*, 231.
(44) Lehrer, F. *Nullfeld-Photoelektronen-Spektroskopie: Entwicklung und Anwendung, Laserspektroskopie und Lasermassenspektrometrie*; Herbert Utz Verlag: München, 1997; Vol. V.